8) Structural materials for fast neutron Generation IV reactors

Intended learning outcomes

After having studied Chapter 8, you will be able to:

1) select operational conditions reducing risk for embrittlement
2) estimate the operational life of fuel cladding materials
3) calculate limiting temperatures of structural materials during transients.

Background

The major risk related to operation of a nuclear power plant is the release to the environment of highly radioactive fission products, in particular ^{131}I. Therefore, the most important requirement for a nuclear power reactor design, is that such fission products shall be retained inside a series of barriers, during nominal operation, as well as under transients. In a liquid metal cooled reactor, these barriers include the fuel cladding tube, the steam generator tube and the primary vessel. The two former are pressurized components and the first is subject to intense radiation damage. Different varieties of steel have been the material of choice for these components in liquid metal cooled reactors, combining strength with ductility. Thanks to a better neutron economy in fast neutron spectra, the relatively high absorption cross section of iron is acceptable.

In this chapter, we will discuss the three major classes of steel that have been used and are considered for fast neutron power reactors. These are austenitic, ferritic and martensitic steels. Whereas pure iron and ferritic steels have a body-centered cubic crystal structure (bcc), austenitic steels are characterized by their face-centered cubic structure (fcc), and are typically obtained by introduction of a sufficient amount of fcc-stabilising elements, such as nickel and manganese. The martensite structure is body-centered tetragonal and is manufactured by rapid quenching (cooling) of an alloy containing a carbon amount above the solubility limit of this element.

Other alloys and even ceramics have been suggested for future applications. However, the applicability of such materials in fast spectrum reactors remains to be proven, and we will not treat them here.

Fuel cladding tubes

During operation, the fuel cladding tube steel will be subjected to various loads of thermo-mechanical origin. Besides thermal stress due to temperature gradients, a phenomenon unique for nuclear fuel applications is the build-up of fission gas pressure inside the tube. As we have seen in the chapter 6, about 80% of all gases produced by fission in oxide an metallic alloy fuels will eventually be released from the fuel to the internal space of the rod, i.e. the gas plenum. As the yield of xenon and krypton in a fission event is 25%, we have that after 10% burn-up, the number of fission gas atoms in the plenum is about 2% of the initial actinide inventory. Knowing that under room temperature conditions, gases occupy a volume three orders of magnitude larger than their solid forms, one can immediately realize that the internal rod pressure should be of the order of 100 bars (10 MPa), if the gas plenum is of similar volume as that of the fuel column. Moreover, in Generation IV reactors, helium is produced due to transmutation of ^{241}Am into ^{242}Cm, which decays by emitting an alpha-particle with a half-life of 162 days. In general, helium is more mobile than the main fission gases, and will be released to the gas plenum at a lower temperature.

Considering that the ratio δ_{clad}/R_{clad} between the cladding tube thickness and radius is about 0.1, we may adopt the thin wall approximation and estimate the resulting Hoop (circumferential) stress on the cladding surface as

$$\sigma_\theta \simeq P_{gas}\frac{\delta_{clad}}{R_{clad}} \simeq 10\ P_{gas}$$

which under the aforementioned conditions is of the order of 100 MPa. Designing the fuel cladding tube, we have to make sure that it will not rupture due to this stress.

Creep

Materials subject to load (e.g. from gas pressure) will deform permanently in a process known as creep [Bailly 1999]. The typical time dependence for the strain under constant load and temperature is illustrated in Figure 8.1 Following a period of rather constant strain rate, the material will suddenly rupture.

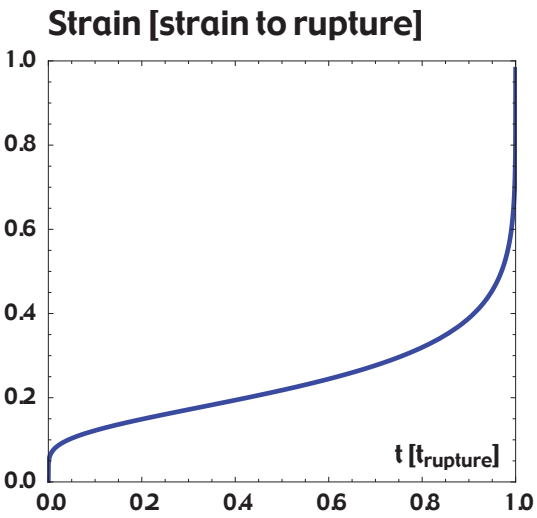

Figure 8.1: Strain versus time, in units of strain and time to rupture.

The relationship between stress, temperature and time to rupture is often expressed as a function of the Larson-Miller parameter [Larson 1952]:

$$\mathrm{LMP} = T\left[C + \log(t_r)\right],$$

where the temperature T is given in Kelvin, the time to rupture t_r is given in hours and the common logarithm has base 10. The formula may be motivated by assuming an Arrhenius type equation for the creep rate:

$$\frac{\Delta l}{\Delta t} = A\exp\left(-\frac{\Delta H}{RT}\right) \rightarrow \frac{\Delta H}{R} = T\left(\ln\frac{A}{\Delta l} + \ln(\Delta t)\right)$$

Where ΔH is a creep activation energy. Hence, the Larson-Miller parameter may be viewed as a measure of the activation energy required to initialize rupture for a given material. Measuring the rupture time for a fixed temperature and stress, the LMP may be used to predict rupture times for other (lower) temperatures, or alternatively, the maximum temperature permitted for the desired life-time of the clad.

Figure 8.2 displays parametrisations of the relation between stress, temperature and time to rupture for two steels that both were optimized for creep resistance: The titanium stabilized austenite 12R72, developed by Sandvik [Wilson 2010, Cautaerts 2017] and the ferritic/martensitic T91 of Oak Ridge National Laboratory [Swindeman 1998, Kimura 2007]. The composition of T91 is compared to that of Sandvik's HT9 in Table 8.1.

Table 8.1: ASTM Standard compositions of T91 and HT9 (wt%). Balance is Fe,

Grade	Cr	Mo	Mn	Si	C	Ni	W	V
T91	8.0-9.5	0.85-1.05	0.4-0.6	0.2-0.5	0.07-0.14			
HT9	11.0-12.5	0.8-1.2	0.4-0.7	0.2-0.3	0.17-0.23	0.3-0.8	0.4-0.6	0.25-0.35

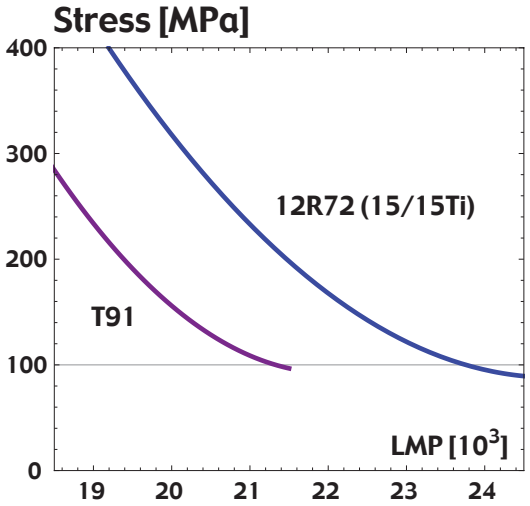

Figure 8.2: Stress-LMP diagram, at point of tube rupture.

Clearly, the austenitic steel has a considerably higher resistance to creep, in spite of austenites generally exhibiting lower yield strength than ferrites and martensites. The difference in Larson-Miller parameter where rupture occurs at a given stress is more than 2000, which corresponds to an increase in rupture life-time by more than a factor of 100.

Let us now assume that the fission gas induced stress in the cladding is 100 MPa. At a peak cladding midway temperature of 850 K, the service life of T91 is still above 50 000 hours (≈ six years). Hence, cladding creep rupture would not be a concern under nominal conditions. However, during a transient, peak temperatures may be substantially higher during a significant time lapse. E.g., at 1070 Kelvin, the rupture life of T91 is reduced to half an hour, while 12R72 (15-15Ti) would still remain intact for over 100 hours. Therefore, austenitic steels were selected as fuel cladding material for most fast neutron power reactors in the world.

Unfortunately, austenitic steels are vulnerable to a phenomenon that is inherent to fast neutron reactors. In 1967, Cawthorne and Fulton discovered that SS316 fuel cladding tubes irradiated in the Dounray Fast Reactor (DFR) suffered from a highly detrimental increase in volume, or swelling [Cawthorne 1967]. The phenomenon turns out to be induced mainly by fast neutrons, and is highly temperature dependent,

Swelling

When fast neutrons interact with the atoms in a metallic crystal lattice, they transfer some of their kinetic energy to the nuclei by elastic and in-elastic scattering. For neutron energies below 1 MeV, we may assume that the scattering is isotropic. The kinetic energy acquired by the so-called primary knock-on-atom (PKA) in an elastic collision may then be approximated by:

$$E_{PKA} = \frac{2m_n m_{PKA}}{(m_n + m_{PKA})^2} E_n \simeq \frac{2m_n}{m_{PKA}} E_n \,.$$

Given that most nuclei in a steel have a mass of 50-60 times that of the neutron, the resulting PKA energy will be 3-4% of the impending neutron energy. As the neutron flux spectrum peaks at a few hundred keV, we have a primary recoil spectrum centered around ten keV.

The energy required for an atom to be permanently displaced from its lattice position depends on the direction of the recoil. In iron, the minimum energy is measured to be 17±1 eV [Maury 1976], and the average has been calculated to be around 40 eV, using several different models for the interaction between iron atoms [Nordlund 2006]. Hence, the average collision between a fast neutron and a nucleus will cause a recoil

cascade involving hundreds of atoms. Eventually, the heat will dissipate, and a majority of the displaced atoms will resettle in proper crystal lattice positions, albeit not the same as the original sites. However, some atoms end up in so called interstitial positions, leaving a vacant site behind. Such pairs of an interstitial atom and a vacancy are called Frenkel pairs, and constitute the basic building blocks of radiation damage.

Figure 8.3 shows how the local lattice structure is modified by production of a Frenkel pair in a ferromagnetic bcc lattice representative for pure iron and ferritic steels. The forces between the interstitial and its nearest neighbors are such that they rearrange into a so-called "dumbbell" configuration, where two atoms share a lattice site.

During irradiation, migrating "point defects" might aggregate into clusters. Vacancy clusters form cavities (voids). Clusters of interstitial atoms may migrate to grain boundaries, effectively leading to a a volume increase and hence swelling of the bulk material.

At low temperatures ($T < T_{melt}/3$) vacancies are immobile, and they will tend to annihilate with migrating dislocation loops, yielding small swelling rates. On the other hand, at high temperature ($T > T_{melt}/2$), re-emission of vacancies makes it impossible for voids to grow large. Consequently, we expect the accelerated swelling phase to be of relevance in a medium temperature range. Unfortunately, this range coincides with the operational regime of liquid metal cooled reactors.

Figure 8.4 illustrates the temperature dependence of swelling in austenitic SS316 steels irradiated to different damage doses in DFR and Phénix.

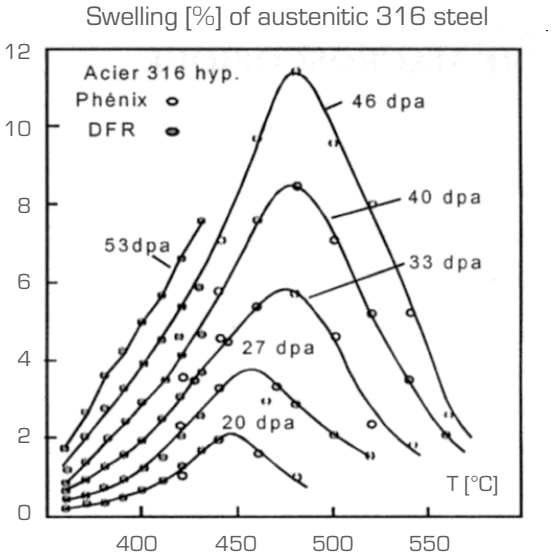

Figure 8.4: Swelling of SS316 steels as function of damage dose and temperature.

A maximum swelling rate is observed between 450-500°C, where the volume increase exceeds 5% for a damage dose of 30 dpa (displacements per atom). A swelling of this magnitude is sufficient for the material to loose its mechanical strength and become brittle.

Here, we need to digress somewhat to clarify the units of damage dose. A simple formula to estimate the number of Frenkel pairs created by a single recoil was suggested by Kinchin and Pease [Kinchin 1955]:

$$\nu_{Frenkel} = \frac{E_{dam}}{2E_{dis}},$$

where the damage energy E_{dam} is slightly lower than E_{PKA} due to losses of energy to ionisation. The displacement threshold energy E_{dis} is the average energy required to displace an atom from its lattice site,

equal to 40 eV in bcc iron. The factor of two derives from the fact that a recoil energy of 79 eV still would only be sufficient to displace one atom permanently.

The Kinchin-Pease formula does not take into account the large amount of interstitial-vacancy recombination events occurring during cooling of a recoil cascade. Early computer simulations made Norgett, Torrens and Robinson to adopt a constant correction factor of 0.8 to the Kinchin-Pease value, thus defining the "NRT" dpa as the *dose obtained when all atoms in a material have been displaced once*, using the approximation [Norgett 1975]:

$$\nu_{NRT} = \frac{0.8E_{dam}}{2E_{dis}}.$$

Unfortunately, these early simulations we're not adequate for the range of PKA energies actually occurring in a fast neutron reactor, where the surviving fraction of point defects later was established to be between 20% and 40% [Pythian 1995]. Furthermore, it turns out that the volume increase under irradiation is not a unique function of of dose as measured in dpa, since the dose rates is essential for determining the swelling of austenitic steels [Budylkin 2004]. However, the field is suck with the NRT standard, and radiation damage dose in nuclear materials is up to the present day most often provided in the unit of dpa. An alternative approach is the of fast neutron fluence, where a damage dose of 50 dpa roughly is equivalent to a fluence of neutrons with an energy above 0.1 MeV equal to 10^{23} neutrons/cm^2 [Garner 2000].

One would desire that a physically more adequate unit could be applied to quantify radiation damage dose. In lieu of such a unit, it is recommended to provide the associated dose rate/fast flux, when comparing the swelling of two materials irradiated to the same damage dose.

Let us now return to swelling. The apparent temperature dependence in Figure 8.4 is actually caused by a temperature dependent threshold from a low swelling regime to an "accelerated" swelling regime, as illustrated in Figure 8.5. Once this transition has occurred, the swelling rate per dose unit is reasonably similar for the whole temperature range. For austenitic steels, this accelerated swelling rate is about 1% per dpa [Garner 1984, Garner 1985, Garner 2000]. Hence, once this regime comes into play, the residual lifetime of the material is short. Therefore, the incubation dose for accelerated swelling to occur is the major parameter determining the service life of fast reactor fuels. As shown in Figure 8.5, the incubation dose for SS316 at T = 720 K may be as low as 20-30 dpa, compared to above 80 dpa when irradiated at 820 K under thee same does rate. Noting that the expected dose rate in an industrial liquid metal-cooled reactor would be of the order of 40 dpa per year, it is desired to develop more swelling tolerant grades of austenitic steels.

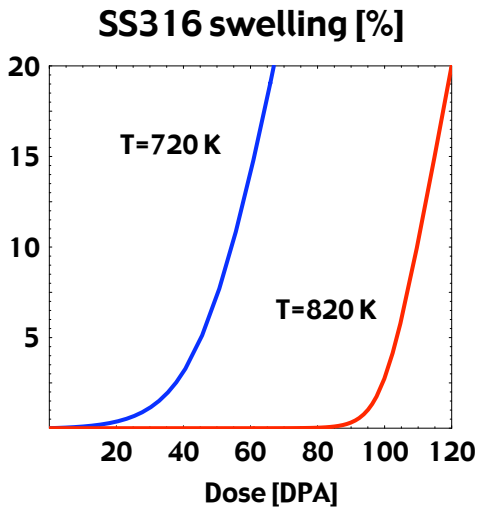

Figure 8.5: Swelling of SS316 steels as function of damage dose and temperature.

To this end, the addition of titanium, silicon and phosphorous have proven to be successful in suppressing swelling [Séran 2016]. These elements acts as inhibitors of swelling as long as they are dissolved into the matrix, where they may trap single vacancies and interstitials that otherwise would be mobile. However, both thermal aging during fabrication and in-pile irradiation may cause them to precipitate into carbides which function as nucleation point of voids.

Finally, by applying 20-30% cold work, in this case by drawing of tubes to their design dimensions, has been shown to improve swelling tolerance. This is explained by an increase in homogeneity of the microstructure, corresponding to fewer sites where nucleation of voids may take place [Séran 2016].

These considerations lead the majority of liquid metal cooled reactor programs to adopt the cold-worked "15-15Ti" grade or variants thereof as reference material for the fuel cladding tube. The composition of this material is provided in Table 8.2. It has been qualified under irradiation in Phénix for an irradiation dose of up to 100 dpa.

Table 8.2: Composition (wt%) of irradiation tolerant austenitic steels. Balance is Fe.

Grade	Cr	Ni	Mo	Mn	Si	C	Ti	P	B
15-15Ti	15.0	15.0	1.3	1.6	0.5	0.1	0.5	0.04	0.006
AIM1	15.0	15.0	1.5	1.5	0.8	0.1	0.4	0.04	0.006

In order to improve the performance beyond 15-15Ti, the fraction of silicon in the AIM1 alloy has been raised to 0.8%. AIM1 is not yet fully qualified, but may permit a damage dose of up to 120 dpa, as illustrated in Figure 8.6.

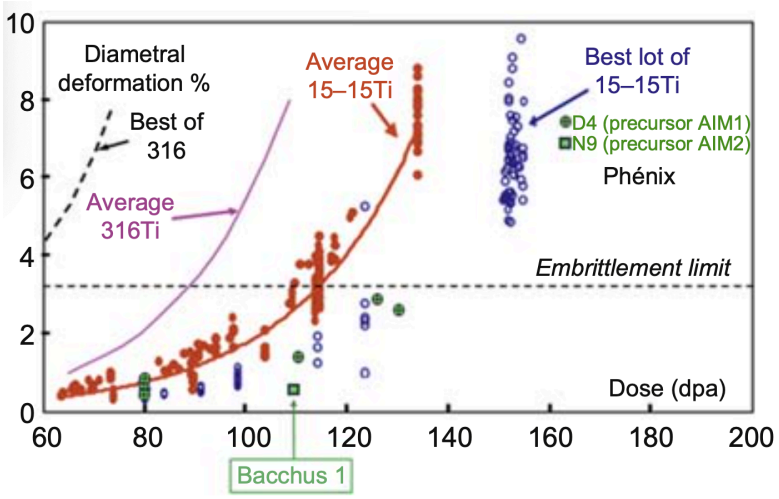

Figure 8.6: Swelling of austenitic steels irradiated in Phénix [Séran 2016].
The D4 alloy is a precursor of AIM1 with slightly higher Si (0.9%) and Ti (0.5%) content.

In terms of experimental alloys, a class of austenites with about 25% Ni appear to exhibit even better tolerance to swelling. The optimum composition and manufacturing route is yet to be determined, but data from the BACCHUS irradiation indicate a swelling lower than that of AIM1 at a damage dose of 110 dpa [Séran 2016].

Ferritic and ferritic/martensitic steels are considerably more resistant to swelling, with a recorded volume increase of 1-3 % at a damage dose of 208 dpa [Toloczko 1994]. The reason for this is not fully understood, but is believed to be related to the difference in dislocation structures and their mobility in bcc and fcc structures, respectively. As we already have discussed, these classes of steel are not suitable for application as fuel cladding tubes, due to their poor creep strength. On the other hand, they may be adequate for structures not having a pressure boundary function, such as fuel assembly hex-cans and grid plates. However, in this

context one must take into account another phenomenon which limits the range of temperatures where a structural material may be used, namely embrittlement.

Embrittlement

Impact toughness refers to the ability of structural materials to remain intact when subjected to very high strain rates. A standardized "Charpy" test may be used to measure the relative impact toughness of materials. The test determines the amount of energy absorbed by the specimens prior to fracture, and is conducted by letting a pendulum axe swing at a notched sample. Performing the tests as function of temperature, bcc and bct materials (but not fcc!) exhibit a transition from a brittle regime where virtually zero energy transfer occurs during fracture, to one where a significant amount of energy is required. The threshold is known as the "ductile to brittle transition temperature", or DBTT. Figure 8.7 illustrates the principle for this transition.

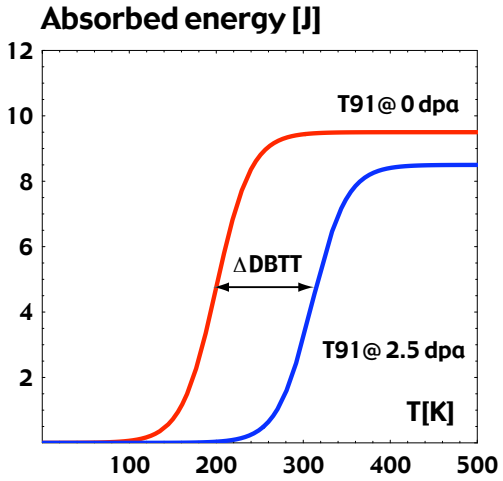

Figure 8.7: Impact toughness as function of temperature for the ferritic/martensitic steel T91 at zero and 2.5 dpa.

While ferritic and ferritic/martensitic steels have an as fabricated DBTT well below room temperature, fast neutron irradiation shifts this threshold towards higher temperatures. In a fission reactor, most of this shift occurs within the first 20-30 dpa, after which the shift will saturate. Figure 8.8 displays the DBTT shift measured for two so called low-activation ferritic/martensitic steels after irradiation at T = 570-600 K in HFR and BOR-60 [Gaganidze 2011]. Note that the shift may be as large as 250 K! Even though this means that the materials remain ductile during nominal operation conditions, they may become brittle during low temperature stand-by conditions, and in particular during discharge from the reactor.

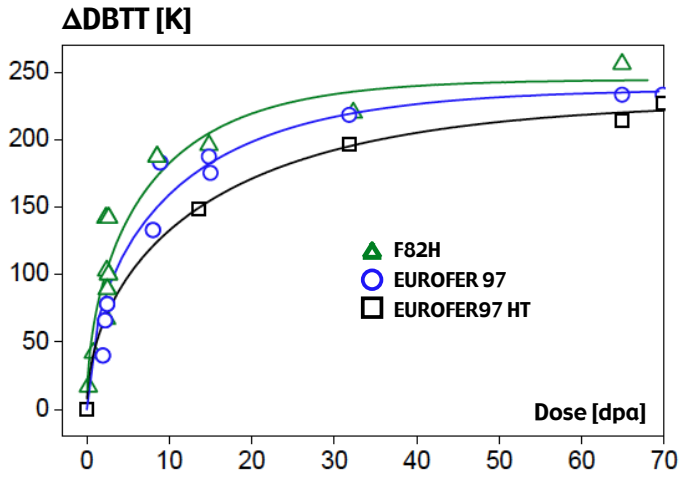

Figure 8.8: Shift in ductile to brittle transition temperature as function of dose after irradiation at T=570-600 K.

One should observe that the magnitude of the shift depends on the irradiation temperature. Figure 8.9 displays data obtained for the low-activation steel EUROFER97 after irradiation to 15 dpa in HFR [Gaganidze 2007]. Above 620 K (350°C) the shift is small, which means that from the perspective of irradiation induced embrittlement, most prototype and industrial liquid metal cooled reactors could make use of such steels for structural components.

The magnitude of the shift does depend on composition, and a minimum in the shift of DBTT is found for 9% [Kohyama 1996]. This is one of the reasons for selecting so-called 9Cr ferritic-martensitic steels for application as wrapper tubes in liquid metal cooled reactors. 12Cr ferritic steels, such as HT9, exhibit a significant DBTT after irradiation at 670 K (400°C) [Séran 1994], which is the operational core inlet temperature for a range of liquid metal cooled reactors.

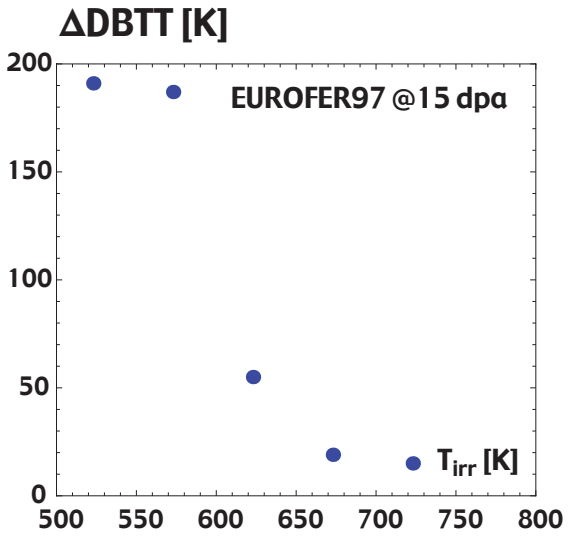

Figure 8.9: Shift in DBTT for EUROFER97, as function of irradiation temperature after a dose of 15 dpa.

The reason for why ferritic steels with a Cr content of 10% and above undergo irradiation embrittlement is believed to be the formation of the alpha-prime phase. Alpha-prime denotes thermo-dynamically stable chromium rich precipitates, which form by thermal diffusion in Fe-Cr alloys if the Cr concentration exceeds the solubility of Cr in bcc-iron [Grobner 1973]. Figure 8.10 shows a computer simulation of such precipitates residing in bulk Fe-Cr [Olsson 2005]. These precipitates function as obstacles for dislocation movement, hence decreasing the ductility of the material.

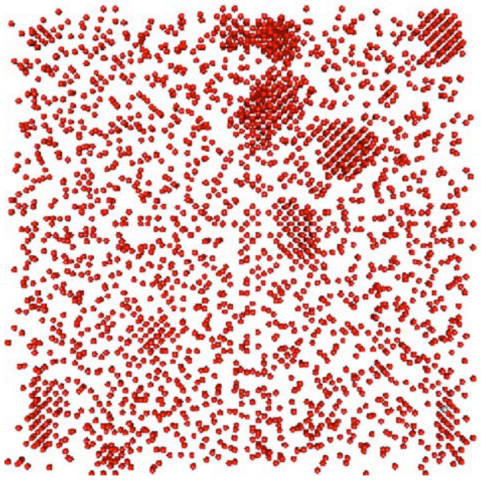

Figure 8.10: α′ (Cr-rich) precipitates simulated to form in Fe-10Cr model alloys after aging at T = 740 K

Historically, it was considered that any solubility of Cr in bcc Fe was due to effects of thermal entropy only, meaning that irradiation assisted precipitation of the alpha-prime phase would have a rather smooth

dependence on Cr concentration, as can be inferred from the published Calphad phase diagram [Andersson 1987].

To the contrary, DFT calculations suggest that the mixing energy of Fe-Cr is negative up to about 10% Cr content, which means that alpha-prime precipitates should not be able to form at lower Cr concentrations, not even under assistance from irradiation [Olsson 2003, Klaver 2006]. A revised phase diagram has been suggested by Bonny and co-workers (see Figure 8.11), correlated to the the sharp increase in irradiation hardening when Cr content exceeds 9% [Bonny 2008].

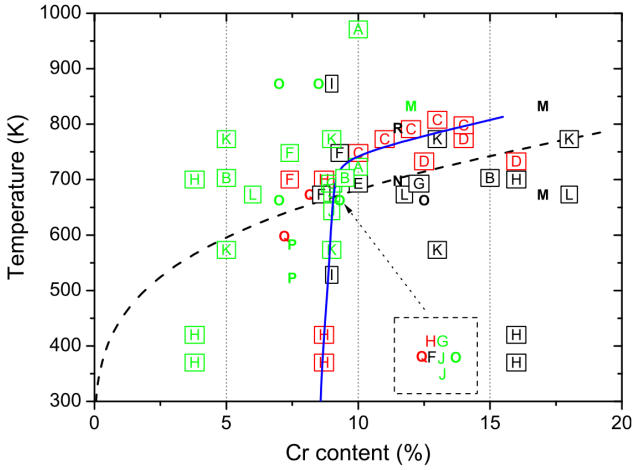

Figure 8.11: $\alpha - \alpha'$ phase boundary. Dashed line: Reference CALPHAD boundary by Andersson. Blue line: modified by Bonny to describe the absence of α' phase formation of Fe-Cr with less than 9% Cr under low T irradiation.

Liquid metal embrittlement

A potentially bigger concern with the respect to the use of bcc and bct materials in contact with liquid metal is the phenomenon of liquid metal embrittlement. It is manifested as an increased propensity for stress induced crack propagation when a solid metal is in contact with a liquid. The effect is measurable in so-called slow strain-rate tension tests, where a specimen is pulled apart with an applied stress adjusted to achieve a constant strain rate, until it starts to plastically deform and eventually fractures. The fracture may be of ductile or brittle character, where the latter implies zero plastic elongation. During the test one can register the yield stress (YS), the ultimate tensile strength (UTS), the elongation ϵ and the reduction in area of the specimen, as illustrated in Figure 8.12.

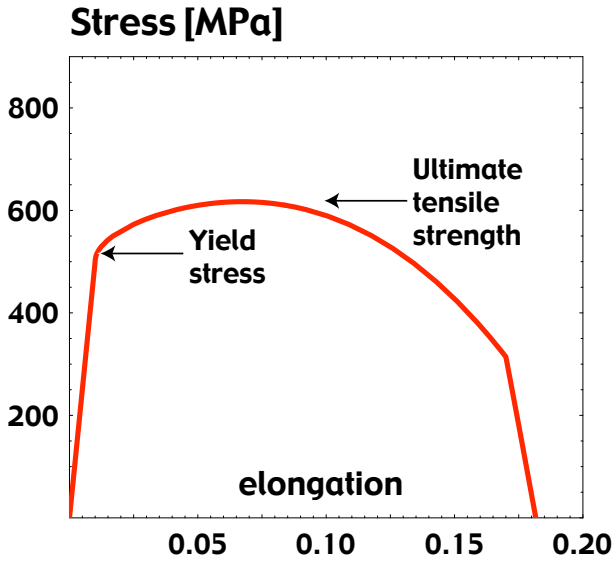

Figure 8.12: Generic stress-strain diagram obtained from a slow strain-rate tensile test.

When performing this test in a liquid metal environment, the elongation of the sample at the point of fracture may be reduced, in a temperature dependent fashion. Figure 8.13 demonstrates how the total elongation of T91 is reduced when performing this test in an LBE environment, for test temperatures below 500°C [Long 2008]. The so-called "ductility through" is deeper and wider the harder the initial state of the sample is. One may note that the samples in all cases retain some plastic elongation and never become totally brittle. At 500°C, there is no effect of the liquid metal environment, but at 450°C it is already significant.

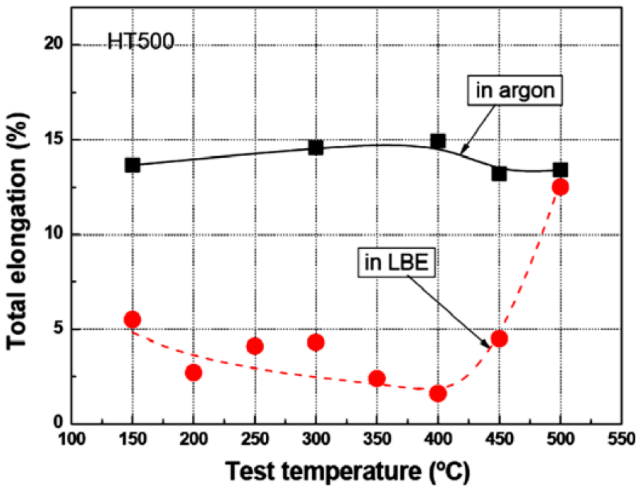

Figure 8.13: Reduction in elongation of T91 when tension tested in lead-bismuth [Long 2008].

Since irradiation in general causes a hardening of the material (that is an increase in yield stress), the effect of irradiation is to enhance liquid metal embrittlement in terms of the depth of the ductility through. However, the threshold for when the chemical environment starts to have an impact on elongation after irradiation does not seem to be affected [Long 2012].

Recent slow strain rate tests of alumina forming ferritic steels in pure lead, as opposed to LBE, indicate an absence of liquid metal embrittlement [Peterson 2021]. It appears as bismuth is the reason for LME of this class of steels, which may be considered as another incentive for selecting lead as reactor coolant, rather than lead-bismuth eutectic.

The risk for LME may be reduced by ensuring that steel surfaces are well protected by a ductile oxide scale. Such an oxide scale is also essential to avoid corrosion attack on thin wall pressure boundaries in lead-cooled reactors.

Corrosion

Corrosion may be defined as any kind of chemical attack on the integrity of a metal alloy, including both dissolution and oxidation. In general, nickel has a higher solubility in liquid metals than do iron and chromium. Below T = 820 K, the solubility of nickel in sodium is sufficiently low that it does not pose a problem. However, oxygen dissolved in the coolant may react with the steel, forming a metal oxide surface layer. A thin layer actually is beneficial for performance, as it protects from dissolution of the cladding into the coolant. However, if this layer grows too thick, it will become detrimental for mechanical and thermo-physical properties of the cladding. One usually requires that the reduction in thickness of the metallic phase of the cladding is restricted to less than 10%, corresponding to 40-50 microns. This criterion can be met in sodium by simply keeping the oxygen concentration low. Typically, it is sufficient to maintain the weight fraction of oxygen below 10 ppb.

The solubility of nickel in lead is considerably higher than in sodium. Figure 8.14 compares the solubilities of Ni, Fe and Cr in lead to those in sodium [Gosse 2014, Fazio 2016]. The solubility of nickel in lead stands out as being orders of magnitude larger. It becomes technologically significant between 400-450°C, pending on the composition of the steel.

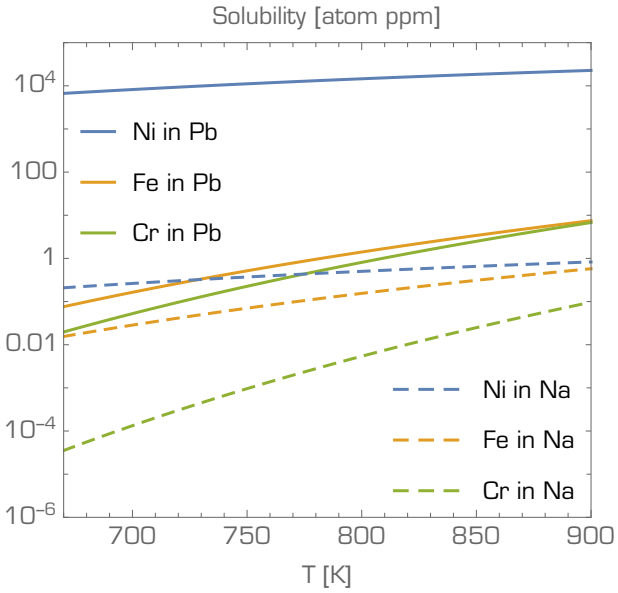

Figure 8.14: Solubility of Ni, Fe and Cr in liquid Pb and Na as function of temperature.

Without a protective oxide scale, nickel dissolution in lead leads to the formation of a ferritic layer on the surface of austenitic steels. For fluid velocities below 1.3 m/s, the corresponding corrosion rate is given by the following expression:

$$v_{cor} = 10^{5.3-2447/T}$$

Where T is given in Kelvin and v_{cor} is obtained in the unit of microns per year [Roy 2012, Fazio 2016]. For a flow velocity exceeding 2 m/s, the corrosion rate can be approximated by:

$$v_{cor} = 10^{3.8-852/T}.$$

At 400°C, the corresponding corrosion rates are 50 and 400 microns/year for low and high fluid velocities, respectively, neither of which are acceptable for a thin walled fuel cladding tube. Hence, this component must always be protected by an oxide scale in a lead-cooled reactor. However, it is not adequate to merely provide a continuous supply of oxygen, since the solubility of oxygen in lead is limited. Once the oxygen concentration exceeds this limit, lead oxide (PbO) will form. In worst case, solid lead oxide particles may cause clogging of coolant channels, leading to reduction of heat removal and eventually fuel failure. As described in Chapter 1, an event of this kind occurred in the first Soviet submarine using lead-bismuth cooled reactors, resulting in a partial core melt and large release of noble gases [Gromov 1997].

Therefore, one must ensure a strict control of oxygen concentration in lead coolants. This oxygen control may be implemented by a combination of measuring the oxygen content using sensors and supplying oxygen by dissolution of PbO pellets [Gromov 1996]. The operation of seven Soviet K705 submarine reactors with LBE coolant showed that this technique is feasible, at least in small size reactors operating at T < 420°C.

The following empirical correlation for the solubility of oxygen in lead has been suggested [Gromov 1998]:

$$C_{sol}(O) = 10^{3.2-5000/T}.$$

Here, the solubility is given in weight percent and the temperature T in Kelvin. Thus, this expression gives us the permissible upper limit for oxygen concentration in the coolant.

Concerning the lower limit, it will depend on the type of oxide that is forming on the surface of the steel. Whereas the change in free energy ΔG^0_{PbO} for formation of PbO is about -280 kJ/mol at 400°C, that of

magnetite, i.e. $\Delta G^0_{Fe_3O_4}$ is -430 kJ/mol. Even more stable are the sesquioxides of chromium ($\Delta G^0_{Cr_2O_3}$ = -650 kJ/mol) and aluminum ($\Delta G^0_{Al_2O_3}$ = -950 kJ/mol). Taking magnetite as the least stable metal oxides that may provide a protective function, we may estimate the lower limit for the oxygen concentration, assuming the following reaction:

$$\frac{3}{4}Fe + PbO \leftrightarrow \frac{1}{4}Fe_3O_4 + Pb$$

For which the free enthalpy can be derived [Fazio 2015]:

$$\Delta G^0_{Fe_3O_4}(T) = -51790 - 21.1T$$

Now, the activity product for formation of magnetite may be written as [Courouau 2004]:

$$a_O a_{Fe}^{3/4} = e^{\frac{\Delta G^0_{Fe_3O_4}}{RT}}$$

where the activities a_O and a_{Fe} are the ratios of dissolved oxygen and iron relative to their respective solubility limit [Courouau 2004]:

$$a_O = \frac{C(O)}{C_{sol}(O)}$$

$$a_{Fe} = \frac{C(Fe)}{C_{sol}(Fe)}$$

Since the condition for the magnetite layer to be stable is that the iron activity in the coolant is $a_{Fe} = 1$, one obtains the minimum required oxygen concentration for this to be ensured as (in units of weight percent):

$$C_{min}(O) > 10^{2.1-8100/T}.$$

Figure 8.15 displays the region of oxygen concentration where a magnetite may form while avoiding precipitation of lead oxides. In a commercial lead-cooled reactor, the operating regime for the fuel cladding surface (including hot shut-down) might be between 690 and 820 K, corresponding to a permissible oxygen concentration range of 1.5x10^{-8} to 3x10^{-5} wt %.

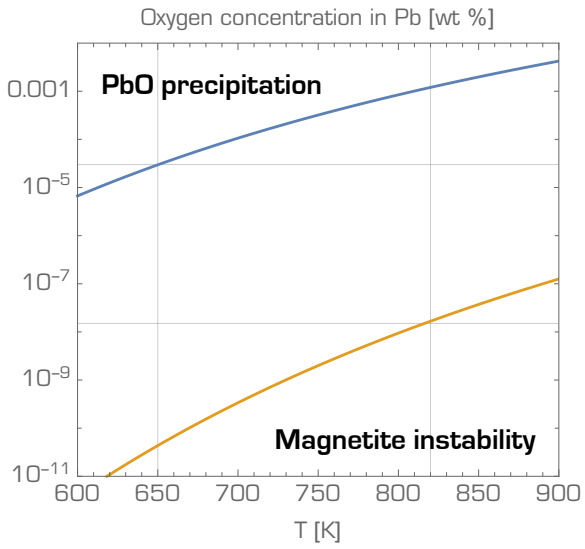

Figure 8.15: Oxygen concentration below which PbO does not precipitate (blue line) and above which magnetite scales form on Fe-Cr and Fe-Cr-Ni steels (orange line).

On Fe-Cr steels, two layers of oxide form on surfaces exposed to lead. An outer, porous magnetite layer, and an inner, protective $Fe_{3-x}Cr_xO_4$ spinel [Martinelli 2011]. The composition of the Fe-Cr-Ni spinel forming on austenitic steels is not well established, yet it appears to be chromium rich. The thickness of magnetite and spinel layers are of similar magnitude, and the growth rate can be describe by a parabolic function. Weisenburger suggests the following expressions for the thickness of oxide scales on T91 and 316L exposed to LBE as function of time and temperature [Weisenburger 2014]:

$$\delta_{T91}(t,T) = (-0.98 + 2.54 \times 10^{-3}T)\sqrt{t}, \text{ valid for } 420°C < T < 550°C,$$

$$\delta_{316L}(t,T) = (-0.31 + 8 \times 10^{-4}T)\sqrt{t}, \text{ valid for } 400°C < T < 500°C,$$

where δ is given in microns T in degrees Celsius and t in hours. Figure 8.16 illustrates the dependence on temperature and time for the oxide scale forming on T91.

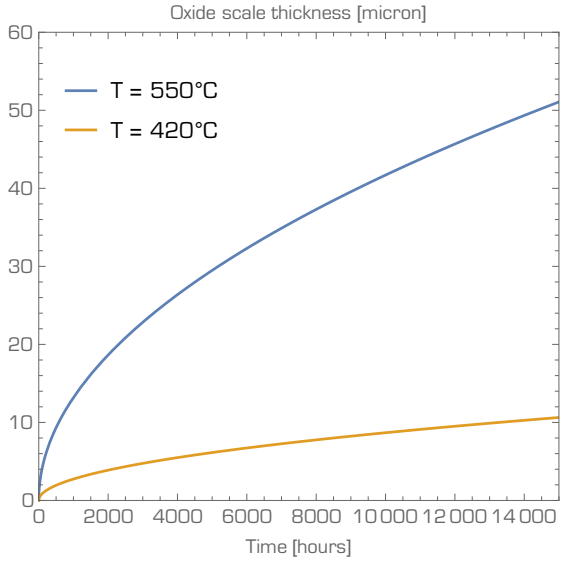

Figure 8.16: Thickness of oxide scales forming on T91 surface exposed to LBE.

Above 550°C (820 K), or below the minimum permissible oxygen concentration, the oxide scales forming on Fe-Cr steels are not stable, and local dissolution attack occurs were scales fail to provide protection. The much thinner scales forming on austenitic Fe-Cr-Ni steels loose their protective properties at T > 450°C or at low oxygen concentration, leading to nickel dissolution attack at defects present in the scales.

Now, since we are limited to austenitic steels as our choice structural material for fuel cladding tubes, a better approach to corrosion protection is required.

The approach taken in Russia is to alloy ferritic-martensitic steels with up to 2 wt% silicon. The protective silicon oxide layer forming under optimal oxygen conditions is both thin and stable up to temperatures of 650°C. Long term tests have shown excellent integrity of the Russian RP-823 steel for exposure times exceeding 60 000 hours at T=870 K (600°C). The embrittling effect of silicon makes it necessary to operate this steel above 420°C and limits the damage dose to about 90 dpa. However, this is considered sufficient for the application of EP-823 as fuel cladding steel for the lead-cooled BREST-300 reactor currently under construction in the region of Tomsk.

In Sweden, alloying of ferritic and ferritic-martensitic Fe-10Cr steels with 4 wt% aluminium and an optimized set of so-called "reactive elements" has resulted in materials with exceptional corrosion tolerance under exposure to lead at both high temperature and low oxygen concentration [Ejenstam 2015, Dömstedt 2019, Dömstedt 2020]. Exposures to stagnant lead with an oxygen concentration of 10^{-7} wt % of Fe-10Cr-4Al-RE for 19 000 hours at 550°C and for 1 760 hours at 800°C resulted in the formation of a very thin, ductile and protective amorphous aluminium oxide. The reactive elements consist of an optimized mixture of Ti, Zr and Nb, which are balanced with respect to the carbon content, for the purpose of eliminating the formation of

metal carbides that may be detrimental for the quality of the protective alumina scale. Whereas this alloy is not mechanically strong enough to serve as a pressure boundary, it may be surface alloyed on 15-15Ti using the pulsed electron beam technique developed by KIT [Müller 2004, Weisenburger 2008], co-extruded with Alloy 800 to serve as corrosion protection for steam generator tubes, or used as weld-overlay on SS316 for pressure vessels. Irradiation tests of model Fe-10Cr-5Al alloys corroborate that that this class of alloys does not suffer from irradiation embrittlement [Fields 2018]. However, it may be vulnerable to liquid metal embrittlement [Chinese paper], and the width of the ductility through remains to be determined. Figure 8.17displays a SEM image of a sample exposed to lead at 800°C for 1760 hours (10 weeks), illustrating the dimension and the quality of the protective scale [Dömstedt 2020].

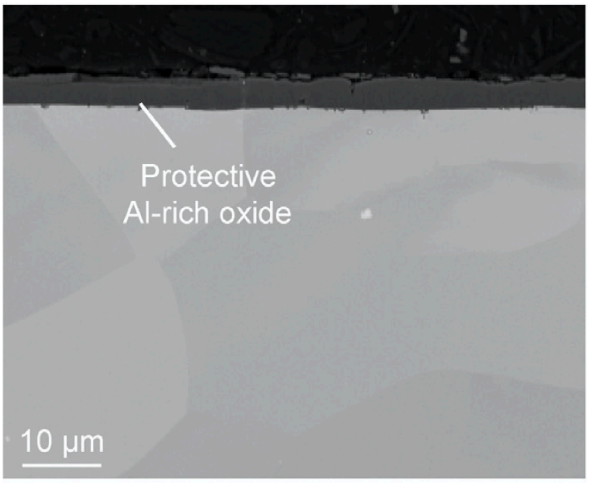

Figure 8.17: Protective aluminium oxide layer forming on Fe-10Cr-4A-RE steel exposed to lead at 800°C.

Exercises:

1) Calculate the time to rupture for ferrite and austenitic steels under nominal and transient conditions.
2) Calculate the maximum permissible temperature for operation thin walled T91 tubes in flowing LBE and low oxygen concentrations.
3) Estimate the oxygen concentration required for Al_2O_3 scales to be stable in liquid lead.

Questions:

1) Which are the conditions under which structural materials become brittle?
2) What are the life-limiting factors for fuel cladding tubes?
3) Which phenomena are safety limiting during transients?

References

Jan-Olof Andersson and Bo Sundman,
Thermodynamic properties of the Cr-Fe system,
Calphad 11 (1987) 83-92.

Henri Bailly, Denise Ménessier and Claude Prunier,
The nuclear fuel of pressurized water reactors and fast neutron reactors,
Lavoisier Publishing, 1999.

Giovanni Bonny , Dmitry Terentyev and Lorenzo Malerba,
On the $\alpha - \alpha'$ miscibility gap of Fe-Cr alloys,
Scripta Materalia **59** (2008) 1193.

N.I. Budylkin et al.,
The strong influence of displacement rate on void swelling in variants of Fe–16Cr–15Ni–3Mo austenitic stainless steel irradiated in BN-350 and BOR-60,
Journal of Nuclear Materials **329–333** (2004) 621–624.

Niels Cautaerts, Remi Delville Wolfgang Dietz Marc Verwerft,
Thermal creep properties of Ti-stabilized DIN 1.4970 (15-15Ti) austenitic stainless steel pressurized cladding tubes,
Journal of Nuclear Materials **493** (2017) 154-167.

C. Cawthorne and E.J. Fulton,
Voids in irradiated stainless steel,
Nature **216** (1967) 575-576.

J.-L. Courouau and J.-C. Robin,
Chemistry control analysis of lead alloys systems to be used as nuclear coolant or spallation target,
Journal of Nuclear Materials **335** (2004) 264–269.

Peter Dömstedt, Mats Lundberg and Peter Szakalos,
Corrosion studies of low-alloyed FeCrAl steels in liquid lead at 750°C,
Oxid. Metals **91** (2019) 511-524.

Peter Dömstedt, Mats Lundberg and Peter Szakalos,
Corrosion studies of a low alloyed Fe–10Cr–4Al steel exposed in liquid Pb at very high temperatures,
Journal of Nuclear Materials **531** (2020) 152022.

Jesper Ejenstam,
Corrosion Resistant Alumina-Forming Alloys for Lead-Cooled Reactors,
PhD Thesis, Kungliga Tekniska högskolan, Stockholm, 2015.

Concetta Fazio, editor,
Handbook on Lead-bismuth Eutectic Alloy and Lead Properties, Materials Compatibility, Thermal-hydraulics and Technologies,
NEA No. 7268, OECD/NEA, 2015.

Concetta Fazio , Fanny Balbaud
Corrosion phenomena induced by liquid metals in Generation IV reactors,
In Structural Materials for Generation IV Nuclear Reactors, edited by P. Yvon, Elsevier Science & Technology, 2016.

K.G. Field et al.,
Radiation tolerance of neutron-irradiated model Fe-Cr-Al alloys,
Journal of Nuclear Materials **465** (2015) 746-755.

F.A. Garner,
Recent insights on the swelling and creep of irradiated austenitic alloys,
Journal of Nuclear Materials **122-123** (1984) 459-471.

F.A. Garner, H.R. Brager and R.J. Puigh,
Swelling behavior of titanium-modified alloys in EBR-II,
Journal of Nuclear Materials **133-134** (1985) 535-539.

F.A. Garner, M.B. Toloczko and B.H. Sencer,
Comparison of swelling and irradiation creep behavior of fcc-austenitic and bcc-ferritic/martensitic alloys at high neutron exposure,
Journal of Nuclear Materials **276** (2000) 123-142.

E. Gaganidze, H.-C. Schneider, B. Dafferner and J. Aktaa,
Embrittlement behavior of neutron irradiated RAFM steels,
Journal of Nuclear Materials **367–370** (2007) 81–85.

E. Gaganidze et al.,
Mechanical properties and TEM examination of RAFM steels irradiated up to 70 dpa in BOR-60,
Journal of Nuclear Materials **417** (2011) 93-98.

S. Gossé,
Thermodynamic Assessment of Solubility and Activity of Iron, Chromium, and Nickel in Lead Bismuth Eutectic,
Journal of Nuclear Materials **449** (2014) 122-131.

P.J. Grobner,
The 885°F (475°C) embrittlement of ferritic stainless steels,
Metall. Trans. **4** (1973) 251-260.

B.F. Gromov and B.A. Shmatko,
Journal of Obninsk, No. 4, IPPE, 1996, No. ISSN 0204-3327.

B.F. Gromov et al.,
Use of lead-bismuth coolant in nuclear reactors and accelerator-driven systems,
Nuclear Engineering and Design 173 (1997) 207-217

B.F. Gromov, Y.I. Orlov, P.N. Martynov and V.A. Gulevskiy,
The problems of technology of the heavy liquid metal coolants (lead-bismuth, lead).
In: Proceedings of the Conference of the Heavy Liquid Metal Coolants in Nuclear Technology, Obninsk, Russian Federation, 5-9 October, 1998, pp. 87–100.

G.H. Kinchin and R.S. Pease,
Rep. Prog. Phys. 18 (1955) 1.

T.P.C. Klaver, R. Drautz and M.W. Finnis,
Magnetism and thermodynamics of defect-free Fe-Cr alloys,
Physical Review B **74** (2006) 094435.

K. Kimura, H. Kushima, F. Abe and K. Yagi,
Inherent creep strength and long- term creep strength properties of ferritic steels,
Material Science and Engineering A, **234-236** (1997) 1079.

A. Kohyama, A. Hishinuma, D.S. Gelles, R.L. Klueh, W. Dietz and K. Ehrlich,
Low-activation ferritic and martensitic stems for fusion applications,
Journal of Nuclear Materials **233-237** (1996) 138.

Frank R. Larson and James Miller,
A Time-Temperature Relationship for Rupture and Creep Stresses,
Transactions ASME **74** (1952) 765–775.

B. Long, Z. Tong, F. Gröschel and Y. Dai,
Liquid Pb–Bi embrittlement effects on the T91 steel after different heat treatments,
Journal of Nuclear Materials **377** (2008) 219–224

B. Long, Y. Dai and N. Baluc,
Investigation of liquid LBE embrittlement effects on irradiated ferritic/martensitic steels by slow-strain-rate tensile tests,
Journal of Nuclear Materials **431** (2012) 85–90

Laure Martinelli, Jean-Louis Courouau and Fanny Balbaud-Célérier,
Oxidation of steels in liquid lead bismuth: Oxygen control to achieve efficient corrosion protection,
Nuclear Engineering and Design **241** (2011) 1288–1294

F. Maury, M. Biget, P. Vajda, A. Lucasson, P. Lucasson,
Anisotropy of defect creation in electron-irradiated iron crystals,
Phys. Rev. B **14** (1976) 5303.

Georg Müller et al.,
Behavior of Steels in Flowing Liquid PbBi Eutectic Alloy at 420-600°C After 4000-7200 h,
Journal of Nuclear Materials **335** (2004) 163-168.

Kai Nordlund, Janne Wallenius and Lorenzo Malerba,
Molecular dynamics simulations of threshold displacement energies in Fe,
Nuclear Instruments and Methods in Physics Research B **246** (2006) 322–332.

M.J. Norgett, M.T. Robinson and I.M. Torrens,
A proposed method of calculating displacement dose rates,
Nuclear Engineering and Design **33** (1975) 50.

P. Olsson, I.A. Abrikosov, L. Vitos and J. Wallenius,
Ab initio formation energies of Fe-Cr alloys,
Journal of Nuclear Materials **321** (2003) 84-90.

P. Olsson, J. Wallenius, C. Domain, K. Nordlund and L. Malerba,
Two-band modeling of α-prime phase formation in Fe-Cr,
Physical Review B **72** (2005) 214119,

Christopher Peterson,
Presentation at SUNRISE meeting,
Uppsala, September 2021.

W.J. Pythian, R.E. Stoller, A.J.E. Foreman, A.F. Calder and D.J. Bacon,
A comparison of displacement cascades in copper and iron by molecular dynamics and its application to microstructural evolution,
Journal of Nuclear Materials **223** (1995) 245-261.

M. Roy,
Mécanisme de dissolution des aciers austénitiques dans l'eutectique Pb-Bi a 500°C,
Ph.D. dissertation, Université Technologique de Compiegne, 2012

J.L. Séran et al.,
Pre- and post-irradiation mechanical properties of ferritic-martensitic steels for fusion applications: EM10 base metal and EM10/EM10 welds,
Journal of Nuclear Materials **212-215** (1994) 588-593.

J.L. Séran and M. Le Flem,
Irradiation-resistant austenitic steels as core materials for Generation IV nuclear reactors,
In Structural Materials for Generation IV Nuclear Reactors, edited by P. Yvon, Elsevier Science & Technology, 2016.

R.W. Swindeman, V.K. Sikka, P.J. Maziasz and D.A. Canonico,
Evaluation of T91 after 130 000 hours in service,
ASME pressure vessels and piping conference, San Diego, July 26-30, 1998.

M.B. Toloczko, F.A. Garner, C.R. Eiholzer,
Irradiation creep and swelling of the US fusion heats of HT9 and 9Cr-1Mo to 208 dpa at ~400°C,
Journal of Nuclear Materials **212-215** (1994) 604–607.

Alfons Weisenburger et al.,
T91 cladding tubes with and without modified FeCrAlY coatings exposed in LBE at different flow, stress and temperature conditions,
Journal of Nuclear Materials **376** (2008) 274-281.

A. Weisenburger, L. Mansani, G. Schumacher and G. Müller,
Oxygen for protective oxide scale formation on pins and structural material surfaces in lead-alloy cooled reactors,
Nuclear Engineering and Design **273** (2014) 584-594.

A. Wilson
Sandvik tubes for nuclear applications
ELECTRA workshop, KTH, 2011.